Available online at www.sciencedirect.com

ScienceDirect

Procedia Structural Integrity 1 (2016) 158–165

Structural Integrity Procedia

www.elsevier.com/locate/procedia

XV Portuguese Conference on Fracture, PCF 2016, 10-12 February 2016, Paço de Arcos, Portugal

Fatigue crack growth in low cycle fatigue: an analysis of crack closure based on image correlation

S. Rabbolini[a,*], S. Beretta[a], S. Foletti[a]

[a] *Politecnico di Milano, Department of Mechanical Engineering, Via La Masa 1, Milan 20156, Italy*

Abstract

In this paper, the effects of crack closure on the propagation of short cracks is investigated. An experimental campaign, performed in the low cycle fatigue regime, was performed on specimens with micro-defects, considering two different strain ratios: initially, tests were performed under fully reversed straining, whereas the effect of an applied mean strain were studied by considering a strain ratio equal to 0.5. Crack closure was characterized with an innovative technique based on digital image correlation: crack opening and closing levels were measured starting from the experimental crack tip displacement fields. Finally, experimental results were compared to those computed with the analytical model proposed by Newman.

Keywords: Low cycle fatigue; Fatigue crack closure; Digital image correlation; Short crack propagation; Fatigue crack growth.

1. Introduction

Modern aviation and energy industry requirements have necessitated the adoption of design techniques based on damage tolerant approaches. In this frame, residual life of components, such as turbine disks and combustors, is evaluated considering a crack propagation problem, in which it is assumed that a crack propagates from the first fatigue cycle, starting from an initial defect present in the component most stressed region (Miller and Murakami (2005)). Accordingly, crack growth rates are calculated with models that take into account low cycle fatigue (LCF) conditions, since cracks usually grow in regions where high plastic strains are present. The natural scatter of the external applied loads is introduced by considering a series of safety factors, calculated following semi-probabilistic approaches (Beretta et al. (2016)). A further improvement in fatigue life assessment can be implemented by considering the presence of small shallow cracks, whose depth is set equal to the detection limit of non-destructive techniques (NDT), as proposed by Cristea et al. (2012).

* Corresponding author. Tel.: +39-02-2399-8248 ; fax: +39-02-2399-8623.
E-mail address: silvio.rabbolini@polimi.it

10.1016/j.prostr.2016.02.022

Nomenclature

R	strain ratio ($\epsilon_{min}/\epsilon_{max}$)
U	stress range reduction factor $\frac{\sigma_{max}-\sigma_{op}}{\sigma_{max}-\sigma_{min}}$
a	crack depth
c	surface crack size
α	constraint factor
ϵ_a	strain amplitude
σ_{cl}	stress at crack closing
σ_{open}	stress at crack opening
σ_{ref}	reference stress for data normalization
σ_{UTS}	ultimate tensile strength
σ'_Y	cyclic yield stress (measured in terms of the 0.2% cyclic proof stress)
σ_0	flow stress

Fatigue crack growth in LCF can be modeled following two different approaches. Apart from models based on the applied plastic strain range (Tomkins (1968)), crack growth rates can be described as a function of the effective cyclic J-integral, ΔJ_{eff}, which is calculated by considering only the part of the fatigue loop when the crack is open (Vormwald and Seeger (1991); Vormwald (2016); McClung and Sehitoglu (1988, 1991)). In the literature, several techniques to measure crack opening and closing levels can be found. McClung and Sehitoglu (1988) characterized crack closure, by adopting the plastic replica technique. In their work, the opening load was evaluated after an accurate analysis of the replicas, taken at different points of the upper branch of the fatigue cycle. A second technique, originally proposed by Vormwald and Seeger (1991), allows the evaluation of crack closure starting from the measurements of strain gages positioned over the cracks. Recent advancements in microscopy and testing equipments allowed the direct observation of crack closure, since it was possible to cycle a specimen in a Scanning Electron Microscope (SEM), as reported by Pippan and Grosinger (2013).

In this work, crack closure was characterized with Digital Image Correlation. Initially, DIC was implemented to measure in-plane displacements of a target surface (Peters and Ranson (1982); Peters et al. (1983); Sutton et al. (1983)). The application of DIC to fracture mechanics and fatigue is due to the pioneeristic works of Riddell et al. (1999) and Sutton et al. (1999), who measured crack opening levels, by tracking the relative displacements of crack flanks during a fatigue cycle. In the following papers published by Carroll et al. (2009) and Pataky et al. (2013), the focus was shifted on strain field present around the crack tip: crack propagation driving forces were extracted fitting experimental displacements with the analytical singular field. This approach was successfully employed even for single crystals, as reported by Pataky et al. (2012) and Rabbolini et al. (2015b). This technique cannot be applied to LCF, since it is based on linear elastic fracture mechanics (LEFM) equations. Therefore, the capabilities of digital strain gages in crack closure characterization are discussed in this work, to provide an accurate description of crack opening levels during propagation in presence of large plastic strains. Finally, experimental results are compared to those calculated with the set of equations proposed by Newman (1981), which is the analytical model usually employed for fatigue life assessment.

2. Experiments

2.1. Material and experimental campaign overview

The steel employed for testing is a grade API 5L X65Q alloy. Full material characterization can be found in the works of Paravicini Bagliani et al. (2013) and Farè et al. (2015). In order to study fatigue crack growth under severe straining conditions, four different loading conditions were considered:

- Strain cycles at R = 0.5 with ϵ_a = 0.0025 mm/mm

- Strain cycles at R = -1 with ϵ_a = 0.0022 mm/mm
- Strain cycles at R = -1 with ϵ_a = 0.0025 mm/mm
- Strain cycles at R = -1 with ϵ_a = 0.0035 mm/mm

2.2. LCF testing

The experimental campaign was performed on axial specimens with a net section of 12 mm x 7 mm. Each sample contained a semi-circular defect, whose depth was set to 0.4 mm. Defects were obtained by Electrical Discharge Machining (EDM).

In order to remove nucleation time from the experiments, before testing, all the experiments were precracked. The compression precracking constant technique, originally proposed by Newman Jr et al. (2005), was adopted in this work. Accordingly, specimens were precracked in compression, with a mean applied stress equal to 200 MPa and a stress amplitude of 200 MPa. It was found that, after 500000 cycles, all the specimens exhibited an average 100 μm long crack extending from both the sides of the EDM notch.

After precracking, specimens were fatigue tested in a servo-hydraulic mono-axial machine: during the tests, applied strain amplitudes were controlled by a longitudinal extensometer and the frequency was set to 0.5 Hz.

A specimen was considered broken when the surface crack extension was equal to 4 mm. After the end of the experiments, all the specimen were broken in liquid nitrogen, to check the shape of the fatigue crack. It was found that all the cracks maintained a semi-circular shape, meaning that, during the experiment, the aspect ratio, a/c, kept constant and equal to 1. An accurate description of the experimental activity can be found in Rabbolini et al. (2015a).

3. Digital Image Correlation for crack tip displacements evaluation

In this work, crack closure was characterized with digital image correlation. The application of DIC requires an accurate preparation of the specimen. Before testing, all the specimens were manually polished to a mirror finish with sand paper, up to a grit of P2500. Measurement surfaces were then airbrushed with black paint, in order to obtain a speckle pattern, necessary to increase the accuracy of the technique.

During test interruptions, necessary to check crack advancement, a fatigue cycle was manually completed, to acquire several image of the defect. An HD digital camera, combined with a 12X lens and a 10X adapter, was employed to take the pictures, with a resolution of 1 μm/pixel. Because of the high magnification and the large displacements involved, it was possible to check only one half of the defect. The minimum number of pictures per cycle was set to 31. Crack tip displacements were calculated by a commercial software, Vic 2D by Correlated Solutions. All the displacements were calculated starting from the reference image, which was the picture taken at the beginning of each measurement cycle, at the minimum applied strain.

Starting from the displacement fields, it was also possible to measure local strains: Lagrange strain tensor equation were employed in this phase. Displacements were locally fitted with a first order polynomial, to obtain smooth results. Crack tip strain evolution during a fatigue cycle for a 1.8 mm long crack tested at R = -1 and ϵ_a = 0.0022 mm/mm are reported in Fig. 3. It should be noted that DIC evaluates the strain field respect to the reference image: this means that the strains depicted in Fig. 3 should be interpreted as the difference between the reference strain field and the one present in the acquired image. Accordingly, DIC measurements are an useful tool for the study of the cyclic zone, the process zone in which reverse yielding occurs.

In Fig. 3a the vertical strain field registered at ϵ = -0.006 mm/mm is reported: a strain gradient around the tip is present, with a maximum strain of 0.0025 mm/mm. The singularity around the tip is more marked at ϵ = 0.0004 mm/mm (Fig. 3b): in this case the maximum vertical strain, measured near the tip, is equal to 0.005 mm/mm. The cyclic plastic zone continuously increases (Figs. 3c and d) and reaches its maximum size at the maximum applied strain, as reported in Fig. 3e. The plastic zone is not symmetric: this is due to the fact that the crack grew at an angle. A main lobe is present, extending from the tip along the direction in which the shear is the maximum. The maximum vertical strain registered during the cycle is higher than 0.016 mm/mm.

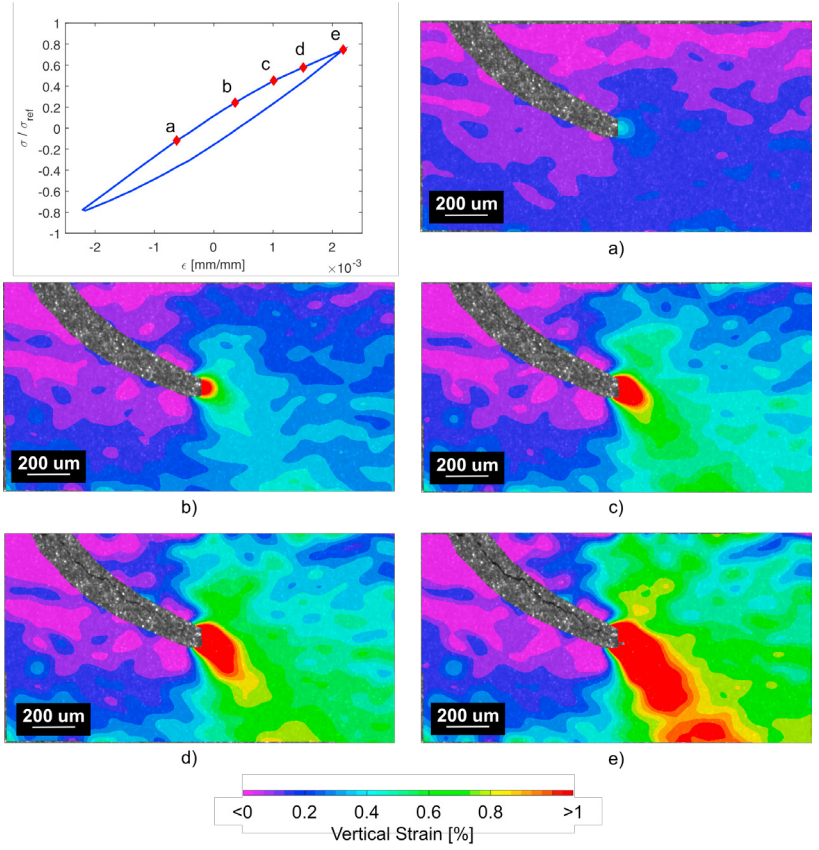

Fig. 1. Vertical strains around the tip of a 1.8 mm long crack in a sample tested at R = -1 and ϵ_a = 0.0022 mm/mm.

4. Crack closure characterization with DIC

In this section, two different methods to measure crack opening and closing levels are presented. The first one, based on digital extensometers, follow the original proposal by Elber (1970), whereas the second method, based on digital strain gages, is a development of the experimental technique proposed by Vormwald and Seeger (1991).

4.1. Digital CTOD

Opening and sliding displacements were measured by two digital extensometers placed across crack flanks, as depicted in Fig. 2a. Gages were placed, respectively, 100 and 200 μm behind the tip. A selected crack tip opening displacements (CTOD) / stress cycle is reported with a blue line in Fig. 2b, in which it can be noted that the experimental stress / CTOD loop presents a hysteretic shape. Crack tip shear displacements (CTSD) are represented in Fig. 2b by a red line: for the given crack length (a = 1.69 mm) shear displacements are higher than crack tip opening displacements. Experimental stresses are presented in normalized form, due to confidentiality issues (i.e. all the stresses were divided by a reference stress, σ_{ref}).

Opening and closing levels (σ_{op} and σ_{cl}) were defined following the offset procedure discussed by Chen and Nisitani (1988) and Skorupa et al. (2002). The part of the CTOD/stress loop, in which loading and unloading branches are not coincident, were linearly fit. Accordingly, the linearized crack mouth opening, $CTOD_{lin}$, was computed as:

$$CTOD_{lin,i} = m\sigma_i + q \tag{1}$$

where m and q are the coefficients of the fitting line. The $offset\ CTOD$ was calculated as:

$$offset \quad CTOD_i = CTOD_i - CTOD_{lin,i} \tag{2}$$

Opening and closing levels were calculated considering the Offset CMOD/stress cycle. Crack opening level was defined as the point in the loading branch whose tangent is parallel to the tangent to the unloading branch, evaluated at the peak stress. Crack closing level was defined as the inflection point of the unloading branch of the CMOD/stress loop. For the given case (Fig. 2c), crack opens when the remote stress is equal to -0.204 , whereas the crack closes with a remote stress equal to -0.536.

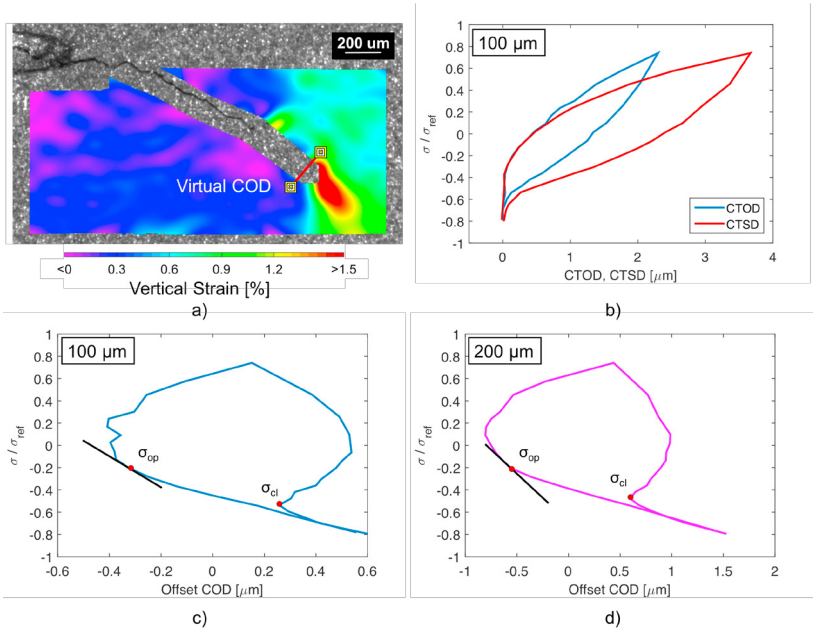

Fig. 2. Crack closure measurements with DIC on a 1.69 mm long crack loaded at R = -1 and ϵ_a = 0.0022 mm/mm. a) Virtual COD position; b) Experimental crack tip opening and shear displacements, 100 μm from the tip; c) crack closure measurement with the offset method, 100 μm from the tip; d) crack closure measurements with the offset method, 200 μm from the tip.

4.2. Digital strain gages

Crack closure levels can be also measured by checking the evolution of the strain field in proximity of a crack tip. Vormwald and Seeger (1991) proposed an experimental technique to measure crack closure during constant strain amplitude tests in the LCF regime based on the local strain concept. During the experiments, local strains are measured by a strain gage positioned as near as possible to a fatigue crack: opening and closing stresses are evaluated as the points in which local and remote behavior start to differ. The change between local and global behavior is associated to the change of local compliance: when the crack is closed, the zone surrounding the crack behaves in the same way of those uncracked regions, whereas a loss in local stiffness is present as soon as the crack starts opening. When the crack is open, global strains are larger than the local ones, since the strain gage measures the strain field in the shadow of the crack.

In this work, a similar approach, based on DIC, is presented. Initially, following the procedure discussed by Vormwald, a 200 μm wide series of digital gages was placed under the EDM notch. Gages were set to read axial strains. A schematic of the strain gage position and the comparison with the remote cycle is reported in Fig. 3, denoted by the label a. This approach does not provide any result, since that part of the specimen does not carry any load. Trying to obtain a correct estimate, the strain gauge was moved in the cyclic plastic zone, very near to crack tip,

as reported in Fig. 3b, where it can be noted that even in this case it is not possible to track opening and closing levels, because of the high plastic strains present.

Finally, the digital strain gage was placed between the cyclic plastic zone and the notch (Fig. 3c): the axial strains measured in this zone can be used to calculate crack opening and closing levels. In order to check the consistency of the proposed method, the gage was moved 50 μm closer to the tip: recorded levels were not affected by this change, confirming the accuracy of the technique. As it can be seen, closing and opening occur at the same strain level, confirming the measurements by Vormwald and Seeger (1991) and the validity of their concept.

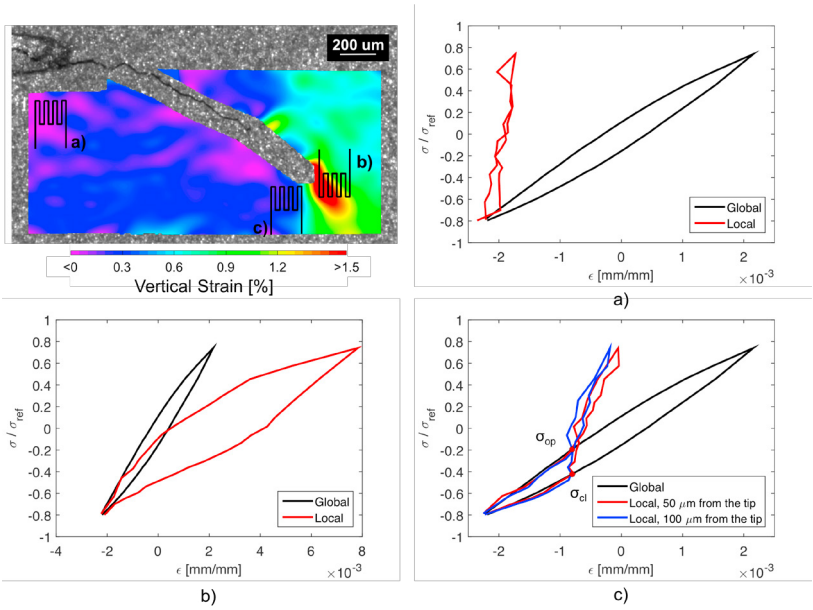

Fig. 3. Crack closure measurements with DIC on a 1.69 mm long crack loaded at R = -1 and ϵ_a = 0.0022 mm/mm, comparison between local and global strains. a) Local strains under the EDM notch; b) Local strains in the cyclic plastic zone; c) Local strains near the tip for crack closure estimation.

5. Results and discussion

The consistency of strain gage measurements was checked by comparing closure levels to those obtained with the CTOD method discussed in the previous section, considering a COD placed 100 μm before the tip. Experimental results, obtained at R = -1 and ϵ_a = 0.0022 mm/mm are reported in Fig. 4 for different crack lengths: both the techniques provide similar results, meaning that the digital strain gage method can be employed to evaluate crack closure effects.

Experimental opening stresses were compared with those calculated with the analytical model presented by Newman (1984), in terms of the stress range reduction factor, U, defined as proposed in Eq. 3:

$$U = \frac{\sigma_{max} - \sigma_{op}}{\sigma_{max} - \sigma_{min}} \tag{3}$$

Newman's model requires the definition of the flow stress, σ_0 and of a constraint factor, α. Initially, the formulation proposed by Vormwald and Seeger (1991) was taken into account. A constraint factor equal to 1, corresponding to a plane stress condition, was considered, since significant out-of-plane constraint is less likely under general yielding (McClung and Sehitoglu (1988)). The flow stress was calculated as the average of the cyclic yield stress, σ'_Y, and of the ultimate tensile strength, σ_{UTS}. In Figure 5a, b and c, experimental results for those tests performed at R = -1 are reported: experimental opening stresses are lower than those analytically calculated, represented in the figures by a blue continuous line. A different formulation of σ_0 was taken into account, to increase model accuracy. Savaidis et al.

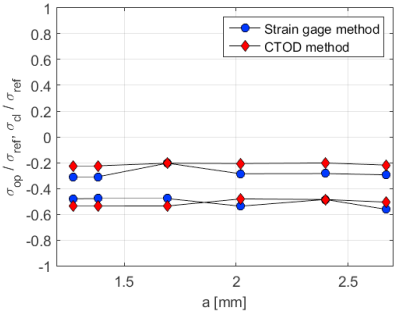

Fig. 4. comparison between the opening and closing stresses measured with the CTOD and the strain gags method at different crack sizes during the experiment performed at R = -1 and ϵ_a = 0.0025 mm/mm.

(1995) proposed to modify the formulation of the flow stress: in their work, Newman's model accuracy was increased by considering the flow stress equal to σ'_Y. The opening levels, calculated following this formulation, are represented in Fig. 5 by a black line. Model accuracy increased in all the considered strain amplitudes, with a very good agreement at ϵ_a = 0.0035 mm/mm. In the case of test at R=0.5 (see Fig. 5d) , the difference between analytical and experimental results is more marked: this shows that the σ_{open} estimates by Newman loose their accuracy at $R \neq -1$. However, it has to be acknowledged in the tests there has been a significant stress relaxation, which is far from the original Newman's assumptions.

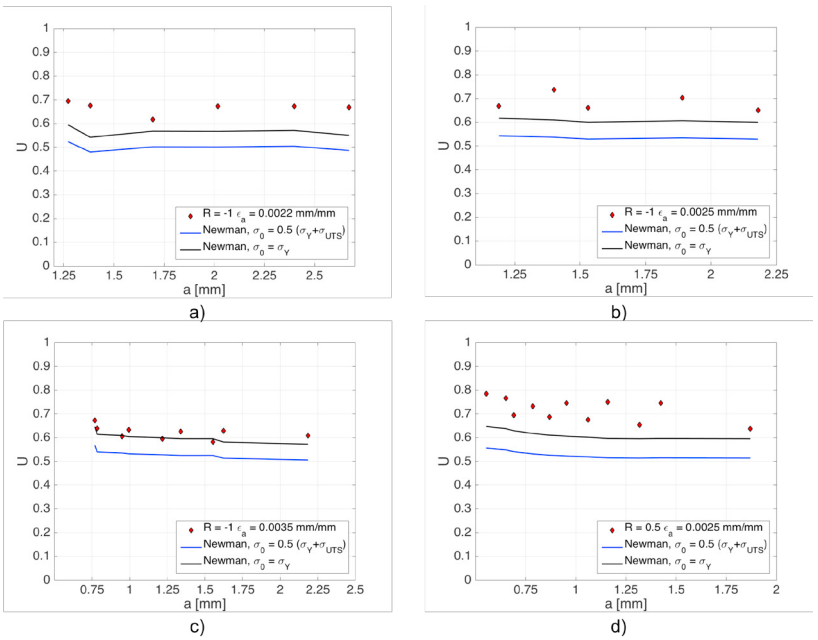

Fig. 5. Comparison between experimental and analytical effective stress amplitudes. a) $R = -1$, $\epsilon_a = 0.0022\ mm/mm$; b) $R = -1$, $\epsilon_a = 0.0025\ mm/mm$; c) $R = -1$, $\epsilon_a = 0.0035\ mm/mm$; d) $R = 0.5$, $\epsilon_a = 0.0025\ mm/mm$.

6. Conclusions

An experimental technique based on DIC was applied to measure crack opening and closing levels during LCF propagation. Crack opening levels could be measured with a digital CTOD as well as with a digital strain-gage near the crack tip, obtaining a good agreement between the two techniques. Moreover, experimental results showed, in

accordance with Vormwald's measurements, that crack opening and closure occur at the remote same deformation level.

The effective stress ranges estimated by Newman's model were close to experiments at R=-1, considering a constraint factor equal to 1 and a flow stress equal to the cyclic yield stress, while predictions at R=0.5 were less precise.

References

Beretta, S., Foletti, S., Rusconi, E., Riva, A., Socie, D., 2016. A log-normal format for failure probability under lcf: Concept, validation and definition of design curve. International Journal of Fatigue 82, 2–11.

Carroll, J., Efstathiou, C., Lambros, J., Sehitoglu, H., Hauber, B., Spottswood, S., Chona, R., 2009. Investigation of fatigue crack closure using multiscale image correlation experiments. Engineering Fracture Mechanics 76, 2384–2398.

Chen, D., Nisitani, H., 1988. Analytical and experimental study of crack closure behavior based on a s-shaped unloading curve. Mechanics of Fatigue Crack Closure 982, 475–488.

Cristea, M., Beretta, S., Altamura, A., 2012. Fatigue limit assessment on seamless tubes in presence of inhomogeneities: Small crack model vs. full scale testing experiments. International Journal of Fatigue 41, 150–157.

Elber, W., 1970. Fatigue crack closure under cyclic tension. Engineering Fracture Mechanics 2, 37–44.

Farè, S., Ortolani, M., Paravicini Bagliani, E., Crippa, S., Novelli, P., Darcis, P., 2015. Mechanical properties and weldability of ultra-heavy wall seamless pipes for sour and arctic-alike environment, in: ISOPE-2015 25th International Offshore and Polar Engineering Conference.

McClung, R., Sehitoglu, H., 1988. Closure behavior of small cracks under high strain fatigue histories, in: Newman, J., Elber, W. (Eds.), Mechanics of FATIGUE CRACK CLOSURE. ASTM. chapter 2, pp. 279–99.

McClung, R., Sehitoglu, H., 1991. Characterization of fatigue crack growth in intermediate and large scale yielding. Journal of Engineering Materials and Technology 113, 15–22.

Miller, K., Murakami, Y., 2005. What is fatigue damage? a view point from the observation of low cycle fatigue process. International Journal of Fatigue 27, 991–1005.

Newman, J., 1981. A crack-closure model for predicting fatigue crack growth under aircraft spectrum loading, in: Chang, J., Hudson, C. (Eds.), Methods and models for predicting fatigue crack growth under random loading. ASTM, pp. 53–84.

Newman, J.J., 1984. A crack opening stress equation for fatigue crack growth. International Journal of Fracture 24, R131–R135.

Newman Jr, J., Schneider, J., Daniel, A., McKnight, D., 2005. Compression pre-cracking to generate near threshold fatigue-crack-growth rates in two aluminum alloys. International journal of fatigue 27, 1432–1440.

Paravicini Bagliani, E., Anelli, E., Paggi, A., Di Cuonzo, S., 2013. Development of heavy wall seamless pipes with improved toughness and hardness control, in: 6th Int Pipeline Technology Conference.

Pataky, G.J., Sangid, M.D., Sehitoglu, H., Hamilton, R.F., Maier, H.J., Sofronis, P., 2012. Full field measurements of anisotropic stress intensity factor ranges in fatigue. Engineering Fracture Mechanics 94, 13–28.

Pataky, G.J., Sehitoglu, H., Maier, H.J., 2013. High temperature fatigue crack growth of haynes 230. Materials Characterization 75, 69–78.

Peters, W., Ranson, W., 1982. Digital imaging techniques in experimental stress analysis. Optical Engineering 21, 213427–213427.

Peters, W., Ranson, W., Sutton, M., Chu, T., Anderson, J., 1983. Application of digital correlation methods to rigid body mechanics. Optical Engineering 22, 226738–226738.

Pippan, R., Grosinger, W., 2013. Fatigue crack closure: from lcf to small scale yielding. International Journal of Fatigue 46, 41–48.

Rabbolini, S., Beretta, S., Foletti, S., Cristea, M., 2015a. Crack closure effects during low cycle fatigue propagation in line pipe steel: An analysis with digital image correlation. Engineering Fracture Mechanics 148, 441–456.

Rabbolini, S., Pataky, G.J., Sehitoglu, H., Beretta, S., 2015b. Fatigue crack growth in haynes 230 single crystals: an analysis with digital image correlation. Fatigue Fract Engng Mater Struct 38.

Riddell, W., Piascik, R., Sutton, M., Zhao, W., McNeill, S., Helm, J., 1999. Determining fatigue crack opening loads from near-crack tip displacement measurements. ASTM SPECIAL TECHNICAL PUBLICATION 1343, 157–174.

Savaidis, G., Dankert, M., Seeger, T., 1995. An analytical procedure for predicting opening loads of cracks at notches. Fatigue & Fracture of Engineering Materials & Structures 18, 425–442.

Skorupa, M., Beretta, S., Carboni, M., Machniewicz, T., 2002. An algorithm for evaluating crack closure from local compliance measurements. Fatigue & Fracture of Engineering Materials & Structures 25, 261–273.

Sutton, M., Wolters, W., Peters, W., Ranson, W., McNeill, S., 1983. Determination of displacements using an improved digital correlation method. Image and vision computing 1, 133–139.

Sutton, M.A., Zhao, W., McNeill, S.R., Helm, J.D., Piascik, R.S., Riddell, W.T., 1999. Local crack closure measurements: Development of a measurement system using computer vision and a far-field microscope. ASTM Special Technical Publication 1343, 145–156.

Tomkins, B., 1968. Fatigue crack propagation - an analysis. Philosophical Magazine 18, 1041.

Vormwald, M., 2016. Effect of cyclic plastic strain on fatigue crack growth. International Journal of Fatigue 82, 80–88.

Vormwald, M., Seeger, T., 1991. The consequences of short crack closure on fatigue crack growth under variable amplitude loading. Fatigue and Fracture of Engineering Materials and Structures 14, 205–25.